HHS Public Access

Author manuscript

J Cyst Fibros. Author manuscript; available in PMC 2024 November 01.

Published in final edited form as:

J Cyst Fibros. 2023 November ; 22(6): 1104–1112. doi:10.1016/j.jcf.2023.08.011.

SNSP113 (PAAG) Improves Mucociliary Transport and Lung Pathology in the Scnn1b-Tg Murine Model of CF Lung Disease

Elex S. Harris[a], **Lea Novak**[b], **Courtney M. Fernandez-Petty**[a], **Natalie R. Lindgren**[a], **Shenda M. Baker**[c], **Susan E. Birket**[a,e], **Steven M. Rowe**[a,d,e]

[a]Gregory Fleming James Cystic Fibrosis Research Center, Univ. of Alabama at Birmingham, Birmingham, AL, USA

[b]Department of Microbiology, University of Alabama at Birmingham, Birmingham, Alabama, USA

[c]Synspira Therapeutics, Inc., Framingham, MA, USA

[d]Department of Medicine, University of Alabama at Birmingham, Birmingham, AL, USA

[e]Departments of Pediatrics, and Cell Developmental and Integrative Biology, University of Alabama at Birmingham, Birmingham, AL, USA

Abstract

Background: Mucus stasis, a hallmark of muco-obstructive disease, results from impaired mucociliary transport and leads to lung function decline and chronic infection. Although therapeutics that target mucus stasis in the airway, such as hypertonic saline or rhDNAse, show some therapeutic benefit, they do not address the underlying electrostatic defect apparent in mucins in CF and related conditions. We have previously shown poly (acetyl, arginyl) glucosamine (PAAG, developed as SNSP113), a soluble, cationic polymer, significantly improves mucociliary transport in a rat model of CF by normalizing the charge defects of CF mucin. Here, we report efficacy in the CFTR-sufficient, ENaC hyperactive, Scnn1b-Tg mouse model that develops airway muco-obstruction due to sodium hyperabsorption and airway dehydration.

Methods: Scnn1b-Tg mice were treated with either 250 μg/mL SNSP113 or vehicle control (1.38% glycerol in PBS) via nebulization once daily for 7 days and then euthanized for analysis. Micro-Optical Coherence Tomography-based evaluation of excised mouse trachea was used to

Steven M. Rowe (CORRESPONDING): smrowe@uab.edu.

Some data from manuscript was previously presented at:
North American Cystic Fibrosis Conference, Virtual, Nov. 2020 in abstract and poster format and titled: “Effects of SNSP113 (PAAG) on Mucus Obstruction in the β-ENaC Murine Model of CF Lung Disease”

Credit Authorship Contribution Statement:
Elex S. Harris: Data curation, Formal analysis, Conceptualization, Investigation, Methodology, Writing. Lea Novak: Data curation, Formal analysis, Investigation, Methodology, Review and editing. Courtney M. Fernandez-Petty: Data curation, Investigation, Conceptualization, Methodology, Review & editing. Natalie R. Lindgren: Formal analysis, Methodology. Shenda M Baker: Conceptualization, Methodology, Resources, Review & editing. Susan E. Birket: Conceptualization, Methodology, Review & editing. Steven M. Rowe: Conceptualization, Funding acquisition, Investigation, Methodology, Project administration, Supervision, Review & editing.

determine the effect on the functional microanatomy. Tissue analysis was performed by routine histopathology.

Results: Nebulized treatment of SNSP113 significantly improved mucociliary transport in the airways of Scnn1b-Tg mice, without altering the airway surface or periciliary liquid layer. In addition, SNSP113 significantly reversed epithelial hypertrophy and goblet cell metaplasia. Finally, SNSP113 significantly ameliorated eosinophilic crystalline pneumonia and lung consolidation in addition to inflammatory macrophage influx in this model.

Conclusion: Overall, this study extends the efficacy of SNSP113 as a potential therapeutic to alleviate mucus stasis in muco-obstructive diseases in CF and potentially in related conditions.

Keywords

Cystic Fibrosis; Muco-obstructive disease; Mucolytic; SNSP113; PAAG; Scnn1b-Tg Mouse; Mucociliary Transport; micro-Optical Coherence Tomography

1. Introduction

Muco-obstructive diseases such as cystic fibrosis (CF), chronic obstructive pulmonary disease (COPD), asthma, and non-CF bronchiectasis are characterized by mucus obstruction which promotes infection, inflammation, and lung damage. Mucus obstruction often results from impaired mucociliary clearance (MCC), promoted by defects in ion and fluid transport, mucus hypersecretion, and/or aberrant properties of mucins, the primary constituent of mucus (1, 2).

Mucins are large polymeric glycoproteins with extensive sialylation and sulfation, imparting them with a strong negative charge (3–5). MUC5B and MUC5AC, the principal gel-forming mucins, form the gel layer of mucus that facilitates airway clearance by mucociliary transport (2, 4, 5). The negative charges on these gel forming mucins play important roles in mucin maturation and transport in coordination with its electrostatic microenvironment. During mucin biogenesis, calcium (Ca^{2+}) shields the negative charges on mucins and stabilizes them in globular form (6, 7). Upon secretion into a bicarbonate- and sodium (Na^{+})-rich environment, Ca^{2+} is sequestered and substituted with monovalent Na^{+} ions (8–10). This, in addition to adequate airway hydration, facilitates the hydration and expansion of mucin required for healthy mucus transport (1, 4, 6, 11). In muco-obstructive diseases, ion-fluid transport and/or the intrinsic electrostatic properties of mucin are defective, leading to aberrant mucin biogenesis and maturation. This leads to hyperviscous and aberrantly adhesive airway mucus, ultimately causing chronic infection, inflammation, and lung damage (1, 12–14). Currently, no mucolytics correct the intrinsic electrostatic defects of mucin that lead to mucus stasis, providing a need for the development of a mucin-correcting therapeutic (2, 15).

We have previously shown that a polycationic polymer, SNSP113 (poly (acetyl, arginyl) glucosamine, PAAG), normalizes the structure of mucin from CF sputum and significantly improves mucociliary transport in $CFTR^{-/-}$ rats and ferrets (16), models of mucus stasis characterized by deficient airway bicarbonate (17, 18). Evidence suggests that SNSP113 normalizes CF mucin by interacting with its negative charges and displacing Ca^{2+},

facilitating the exchange of Ca^{2+} for Na^{+} and ultimately compensating for the lack of bicarbonate (16, 19). Here, we evaluated this mucolytic in a Scnn1b transgenic (Tg) mouse model that overexpresses the β subunit of the epithelial Na+ channel βENaC), exhibiting impaired mucus clearance resulting from airway dehydration driven by Na^{+} deficiency, rather than bicarbonate deficiency altering pH. In Scnn1b-Tg mice, mucus stasis occurs through Na^{+} hyperabsorption due to overexpression of the ENaC β subunit rather than to mutant or knockout CFTR (20, 21). We hypothesized that 1) the electrostatic properties of SNSP113 would correct mucus transport and ameliorate lung pathology in a bicarbonate-sufficient, Na^{+-} and fluid-deficient Scnn1b-Tg mouse model of lung disease; 2) even under sufficient bicarbonate conditions, such as in the Scnn1b-Tg mouse, Na^{+} deficiency would be adequate to prevent sufficient Ca^{2+}/ Na^{+} exchange, preventing mucin hydration and expansion; and 3) SNSP113 would aid in this exchange, as it did in the CFTR-deficient models, ultimately improving Scnn1b-Tg mucus stasis and lung pathology. We show that SNSP113 improves mucus transport and lung pathology in a model with functional CFTR but severe airway dehydration.

2. Methods

2.1. µOCT Imaging

Measurements of the functional microanatomy of freshly excised mice tracheas were performed using micro-optical coherence tomography (µOCT), a high-speed, high-resolution microscopic reflectance imaging modality, as previously described (22). For consistency, tracheas were placed in the same proximal-to-distal orientation and the imaging beam was placed at six standardized locations along the ventral surface of each trachea. Ciliary beat frequency (CBF) was investigated by Fourier analysis of the reflectance due to beating cilia using MATLAB (23).

2.2. Bronchoalveolar Lavage

Mice were euthanized via isoflurane inhalation followed by exsanguination per IRB protocol. Two milliliters of PBS were pushed into lungs via 2 separate 1mL syringes and collected in 1mL increments. Bronchoalveolar lavage fluid (BALF) collections were pooled and spun at 210 relative centrifugal force (x g) for 5 minutes. The supernatant was discarded, and cells were resuspended into 1mL PBS. 200uL of cell suspension was added to a cytospin column and spun at 500g for 5 minutes. After drying, slides were stained with Diff-Quick kit (Siemens Medical Solutions, Inc, Malvern, PA). Total white blood cells, macrophages, and neutrophils were counted manually.

2.3. Histopathology

Tracheas and lungs were immersion fixed in 10% neutral buffered formalin and submitted to histology laboratory for tissue processing, paraffin embedding, and sectioning. Tissue sections were stained with hematoxylin and eosin (H&E) or alcian blue-periodic acid Schiff's (AB-PAS). Images were taken at 100X-400X magnification with an Olympus DP25 camera (Tokyo, Japan) using an Olympus BX40 microscope. Quantifications of epithelial height and goblet cells were performed using the entire mucosal area of the bronchi for each animal. Trachea and bronchioles were not included in these analyses.

Epithelial height was measured in multiple regions within the cross sections of the bronchi for each animal using ImageJ (NIH) software. Goblet cells were identified by their dark blue mucin staining by AB-PAS and quantified by counting the number of goblet cells over a given length of multiple bronchi cross sections for each animal. The hilar region of the airway was not specifically evaluated. The occurrence of eosinophilic crystalline pneumonia (ECP) was determined by the presence of eosinophilic crystals and macrophages. Percent ECP lung consolidation was quantified by measuring the area of consolidation with the presence of ECP over the whole lung area. Lungs from lavaged and non-lavaged mice were included in histopathology analysis, noting they were equally represented between treatment groups. Whole lobe scans were performed at 40X magnification using a Biotek Lionheart FX Automated microscope (Agilent, CA). Histologic and morphometric evaluation was performed by a board-certified surgical pathologist (L.N.).

2.4. Myeloperoxidase Quantification

Whole lobes were added to 500uL PBS and homogenized using Tissuelyser II (Qiagen, Hilden, Germany). Homogenate was centrifuged at 820 x g, and supernatant was collected. Myeloperoxidase (MPO) concentration was determined by RD Systems Murine MPO ELISA kit (R&D Systems Inc., Minneapolis, MN).

2.5. Scnn1b-Tg Mouse Model

Scnn1b-Tg mice were derived on a mixed background (C3H/HeN:C57BL/6N) and genotyped as previously described (21). Founder line 6608 was utilized for this study. All experiments used age- and sex-matched Scnn1b-Tg mice or their littermate wild-type (WT) controls. All animal care and procedures were approved by the UAB Institutional Animal Care and Use Committee and performed according to the principles outlined by the Animal Welfare and NIH guidelines for the care and use of animals in biomedical research.

2.6. Drug Administration

Mice were distributed equally among two separate nebulizing chambers, each with a PARI Vios Pro nebulizer (PARI Respiratory Equipment Inc., Starnberg, Germany) fitted to an opening in the chamber sides. Equal volumes of 250ug/mL SNSP113 in phosphate buffered saline (PBS) with 1.38% glycerol in PBS or PBS with 1.38% glycerol in PBS alone (Synspira Therapeutics Inc, MA, US) were added to the nebulizers. Mice were nebulized under constant saturation for one hour, daily for a total of 7 days.

2.7. Statistical Analysis

Statistical analyses were performed in Graphpad Prism (GraphPad, CA, US) version 9.0 or later. Comparisons were made using nonparametric one-way ANOVA using Kruskal-Wallis test followed by Dunn’s multiple comparison test or Ordinary one-way ANOVA followed by Tukey’s to compare individual groups. Fisher’s exact test was used to assess ECP occurrence. P-values < 0.05 were considered significant. Statistics are presented as mean ± SEM unless noted otherwise.

3. Results

3.1. SNSP113 restores mucus transport in Scnn1b-Tg mice without impacting airway hydration.

We previously established that SNSP113 improves MCC in CFTR$^{-/-}$ rats by correcting mucin through an electrostatic mechanism that aids in divalent cation release from MUC5B, allowing subsequent linearization of the protein to a more mature form (16). We hypothesized that SNSP113 would also correct mucociliary transport in an airway surface fluid deficient Scnn1b-Tg mouse model of mucus stasis, since the relative absence of Na+ may defer normal cationic exchange from Ca^{2+} to Na^{+}. To evaluate the effect of SNSP113 on mucociliary transport, Scnn1b-Tg mice were nebulized with 250ug/mL SNSP113 in glycerol vehicle or glycerol vehicle alone daily for 7 days. Three hours following the last treatment, tracheas were excised and imaged via μOCT, a real-time imaging modality that visualizes the functional microanatomy of the airway surface (22, 23). As seen in the representative μOCT images (Figure 1A–C) and confirmed by quantification (Figure 1D,E), ASL but not PCL depth was partially diminished in Scnn1b-Tg vs. WT mice; however, no meaningful difference was seen with vehicle or SNSP113, as expected based on the proposed mechanism of action and indicating that SNSP113 did not significantly impact airway hydration, as reported in CF rats (16). There was also no meaningful difference detected in ciliary beat frequency (CBF) between WT mice or Scnn1b-Tg mice treated with vehicle or SNSP113 (SI Figure 1A). In contrast, SNSP113 (Video 3; Figure 1H) increased transport of particles within the mucus layer of Scnn1b-Tg mice compared to vehicle (Video 2; Figure 1G), significantly improving MCT rate (Figure 1I; SNSP113, 0.96 ± 0.23 mm/min; vehicle, 0.32 ± 0.08 mm/min; $P < 0.05$) to rates seen in WT mice (Video 1; Figure 1F,I; 0.94 ± 0.15 mm/min).

Control tracheae from WT and Scnn1b-Tg mice without nebulization were assessed via μOCT to compare airway physiology at baseline. As observed in the representative μOCT images (Figure 2A,B), Scnn1b-Tg mice without vehicle nebulization exhibited significantly lower ASL (Figure 2C; Scnn1b-Tg, 7.9 ± 0.25 μm; WT, 10.8 ± 0.79 μm; $P < 0.05$) and PCL depths (Figure 2D; Scnn1b-Tg, 4.99 ± 0.06 μm; WT, 5.61 ± 0.11 μm; $P < 0.01$) compared to WT. In addition, compared to WT, Scnn1b-Tg mice showed significantly reduced MCT (Figure 2E–G; Scnn1b-Tg, 0.17 ± 0.06 mm/min; WT, 0.75 ± 0.15 mm/min; $P < 0.05$). The MCT deficit in Scnn1b-Tg mice remained present after nebulization, although the ASL and PCL deficit were normalized, indicating that SNSP113 can increase mucociliary transport by a mechanism independent of airway hydration in a Scnn1b-Tg model of CF, consistent with its proposed electrostatic mechanism.

3.2. SNSP113 reduces goblet cell metaplasia and epithelial hypertrophy in the airways of Scnn1b-Tg mice.

Based on our finding that SNSP113 partially restores mucus transport in Scnn1b-Tg mouse trachea, we hypothesized that SNSP113 would also resolve secondary goblet cell metaplasia and epithelial hypertrophy, which are present in Scnn1b-Tg mice due to aberrant MCC and persist into adulthood (20, 24). Goblet cell metaplasia and epithelial hypertrophy further exacerbate mucus abnormalities and excess mucus production in CF (25–27). To

evaluate this, we nebulized Scnn1b-Tg and WT control mice with SNSP113 or vehicle for 7 days and collected lungs for histopathologic evaluation. Whole lung sections were stained with AB-PAS to visualize the airway epithelium and mucin packed goblet cells in large airways. Representative lung sections at 100X and 400X magnification showed more goblet cells with evident mucin expression per mm of epithelium length and increased epithelial height (Figure 3B), a marker of epithelial injury, in similarly sized airways in vehicle-treated Scnn1b-Tg mice vs. WT mice (Figure 3A). A substantial decrease in goblet cell number and a reduced epithelium was observed in SNSP113-treated Scnn1b-Tg mice (Figure 3C). Quantifications revealed significantly fewer goblet cells per length of airway in SNSP113-treated (55.8 ± 7.0 cells/mm; Figure 3D; $P<0.001$) vs. vehicle-treated (119.0 ± 5.7 cells/mm) Scnn1b-Tg mice, with levels similar to WT mice (59.9 ± 8.2 cells/mm; Figure 3D). SNSP113 also significantly reduced epithelial height (15.15 ± 0.66 μm; Figure 3E; $P<0.01$) vs. vehicle (24.09 ± 1.41 μm) in Scnn1b-Tg mice, restoring the epithelium to a height similar to WT mice (13.45 ± 0.94 μm; Figure 3E). Overall, the reductions in goblet cell metaplasia and epithelial hypertrophy seen with SNSP113 provide evidence that the correction of mucus transport in the Scnn1b-Tg mouse lung subsequently improves secondary lung histopathological changes due to aberrant mucociliary clearance.

3.3. SNSP113 reduces incidence of ECP in Scnn1b-Tg mice.

Scnn1b-Tg mouse lungs exhibit transient macrophage influx and eosinophilic inflammation, as well as chronic neutrophilia (20, 24, 28). We hypothesized that SNSP113 would further improve lung inflammation. Eosinophilic crystalline pneumonia (ECP) is a common pulmonary lesion with a high prevalence in mice with a C57BL/6 background, characterized by brightly colored eosinophilic crystals within macrophages and/or alveolar spaces (29). ECP can occur spontaneously in the presence of other pathologic features such as hyperplasticity, and can be a cause of mortality when comorbid with lung disease that prevents proper clearance of alveolar exudate, due to an accumulation of macrophages (30). Eosinophilic crystal formation has been previously reported in younger Scnn1b-Tg mice and has been shown to accompany inflammation in the Scnn1b-Tg model (24). Interestingly, in our aged mice, we observed that adult Scnn1b-Tg mice at least 16 weeks of age exhibited an increased occurrence of ECP; 6 of 11 vehicle-treated Scnn1b-Tg mice had ECP, whereas zero WT mice were affected (Figure 4D, $P < 0.01$). Interestingly, significantly fewer Scnn1b-Tg mice had ECP occurrence after treatment with SNSP113, with only a single mouse showing mild pneumonia (Figure 4D, $P<0.05$). To quantify the severity of ECP, we measured the total amount of pneumonic consolidation over whole lung area in HE-stained whole lung sections. There was no consolidation in WT mice, but areas of lung consolidation were frequent in Scnn1b-Tg vehicle-treated mice (12.27 ± 4.54 %Consolidation; Figure 4A,B,E; $P<0.01$) yet almost completely absent in Scnn1b-Tg mice treated with SNSP113 (0.10 ± 0.10 %Consolidation; Figure 4C,E; $P<0.05$). Control tracheae from WT and Scnn1b-Tg mice without nebulization were evaluated for the presence of ECP to compare airway physiology at baseline. We observed that non-nebulized adult Scnn1b-Tg mice (8-10 weeks of age) exhibited an increased occurrence of ECP; 4 of 5 Scnn1b-Tg mice exhibiting at least some ECP, whereas zero WT mice were affected (SI Figure 2A–C, $P<0.05$). The total area of pneumonic consolidation of the Scnn1b mice was less than that observed in our nebulized groups (data not shown), likely due to the younger age of the

non-nebulized mice. To evaluate the effect of SNSP113 on immune cell infiltration, BALF was collected from mice after nebulization with 250ug/mL SNSP113 or glycerol vehicle daily for 7 days and total white blood cells (WBCs) and differential counts for macrophages and polymorphonuclear neutrophils (PMNs) were measured. As expected, total WBS count was significantly elevated in vehicle-treated Scnn1b-Tg mice (98.7 ± 18.9 WBC; Figure 4F; $P<0.05$) vs. vehicle-treated WT mice (32.1 ± 7.5 WBC). SNSP113 decreased the total WBC count, but this finding was not statistically significant. The total number of macrophages in the BALF were significantly elevated in vehicle-treated Scnn1b-Tg mice (57.8 ± 11.7 macrophages; Figure 4G; $P<0.01$) vs. vehicle-treated WT mice (11.4 ± 2.9 macrophages) and significantly reduced after SNSP113 treatment (26.2 ± 4.7 macrophages; Figure 4G; $P<0.05$). We did not detect any differences in % macrophages compared to total WBC (SI Figure 2D), most likely due to macrophages being the predominant cell type. Total PMN count was significantly elevated in vehicle-treated Scnn1b-Tg mice (8.5 ± 2.8 PMN; Figure 4H; $P<0.01$) vs. vehicle-treated WT mice (0.33 ± 0.28 PMN). Similarly, % PMN count was significantly higher in BALF of vehicle-treated Scnn1b-Tg mice (8.13 ± 1.89 %PMN; SI Figure 2E; $P < 0.05$) vs. vehicle-treated WT mice (1.29 ± 1.13 %PMN), and SNSP113 had no significant effect on % PMNs in Scnn1b-Tg mice vs. vehicle (9.00 ± 1.97 %PMN). In addition, MPO levels from homogenized lung tissue were significantly elevated in Scnn1b-Tg mice (184.7 ± 19.54 units; SI Figure 2F; $P<0.01$) vs. WT (105.8 ± 8.96 units), but there were no significant differences upon SNSP113 treatment. Together, these data support the improvement in macrophage and total WBC inflammation in the BALF, consistent with resolution of ECP.

4. Discussion

CF is an archetypal muco-obstructive lung disease hallmarked by impaired MCC, a feature common to other diseases (13, 26, 31). Current mucolytic therapies such as rhDNAse and N-acetyl cysteine that aim to improve MCC show only marginal efficacy and do not correct the underlying defect in mucin structure and function (2, 32). We have previously shown that a polycationic polymer, SNSP113, normalizes aberrant mucin structure apparent in CF, improving mucus viscoelasticity and transport in $CFTR^{-/-}$ rats (16). $CFTR^{-/-}$ rats display delayed MCC due largely to the absence of CFTR-mediated bicarbonate transport, and thus SNSP113 represented a novel mechanism of action (17). Here, we have shown that SNSP113 augments MCT and lung pathology in CFTR-sufficient Scnn1b-Tg mice that exhibit severe airway dehydration.

Scnn1b-Tg mice enable evaluation of mucus stasis caused by sodium depletion of the airway surface through hyperactive ENaC activity (20, 21). This results in airway dehydration and mucus hyperconcentration, rather than mucus stasis caused by deficient CFTR-dependent bicarbonate and chloride secretion (33). We show that Scnn1b-Tg mice have significantly diminished ASL, PCL, and MCT at baseline and prior to any nebulized treatment (Figure 2). Nebulization by the glycerol in PBS vehicle increased ASL and PCL in Scnn1b-Tg mice to near WT levels. On the contrary, MCT was only marginally increased (from 0.17 to 0.32 mm/min), with a significant remaining deficit of 0.62 mm/min compared to WT, which was only restored after nebulization with SNSP113. The increases in ASL and PCL after vehicle nebulization of Scnn1b-Tg mice were likely due to the acute increase in hydration by PBS, a

reduced discrimination between vehicle treated WT mice. This is consistent with a previous report that showed and acute increase in mucus layer height after administration of isotonic saline, which was exaggerated in Scnn1b-Tg mice (34). Furthermore, this report showed that neither hypertonic saline nor bicarbonate improved mucus transport compared to isotonic saline, although hypertonic saline did increase the mucus layer height. The findings in this report complement findings in the current study while highlighting the potential benefit of SNSP113 in this model.

As expected, SNSP113 did not alter ASL or PCL beyond vehicle, indicating correction of mucus transport independent of airway hydration, as seen in $CFTR^{-/-}$ rats (16). Noting this consistency between models, we propose a consistent mechanism: mucus transport is likely augmented by displacing Ca^{2+}, facilitating the exchange of Ca^{2+} for Na^{+} within MUC5B molecules, and subsequently promoting mucin expansion to a less viscous state (6, 11, 16). Although Scnn1b-Tg mice are not deficient in bicarbonate, which is proposed to actively chelate Ca^{2+} ions to facilitate their de-aggregation from MUC5B (8, 9), the affinity of SNSP113 due to positive arginine moieties to the negative charges in mucin may favor Ca^{2+} displacement; this augments its exchange for Na^{+} when positive counter ions may be less available, as we speculate could occur in this model of airway dehydration (10, 19). Since SNSP113 is a highly charged polymer, and previous work demonstrates that it closely associates with MUC5B in a Ca^{2+}-dependent fashion, SNSP113 likely increases the hydrophilicity of mucin and facilitates its expansion. Mechanistic studies evaluating the macromolecular forms of mucin in this model of airway sodium depletion alongside treatment with SNSP113 are needed to validate this concept. Prior in vitro studies showed that the effect of SNSP113 (i.e. PAAG) on mucus viscosity were observed within 24 hours of treatment (16). We hypothesized longer treatment would likely be needed to rectify mucus transport in vivo, and designed our studies accordingly; thus we are unable to discern whether the kinetics of the beneficial effect on mucociliary physiology of SNSP113 could be more rapidly observed *in vivo*. Regardless, the ability of SNSP113 to restore MCT in Scnn1b-Tg mice provides clear evidence that SNSP113 may have therapeutic efficacy as a mucolytic in many disease states characterized by defects in mucus viscosity due to aberrant electrostatics properties of MUC5B.

This study highlights the ability of SNSP113 to improve secondary lung pathology by significantly reducing airway epithelial hypertrophy and goblet cell metaplasia, common features of muco-obstructive disease that exacerbate lung pathology by increasing mucus production and contributing to airway obstruction (26, 27). Unfortunately, we did not observe prominent mucus plugging in our Scnn1b-Tg mice as previously reported. This was likely due to variability among strains and age of mice mice, and possibly because the hilar region of the lung, where prominent mucus plugging has been previously reported during histopathological analysis, was included but not featured in our study (35). However, we did observe significant increases in epithelial height and goblet cells in our Scnn1b-Tg mice (Figure 3). It has been reported that goblet cell metaplasia occurs after the development of muco-obstruction in Scnn1b-Tg mice, and therefore, occurs as a response to impaired MCC (20, 36). This study showed that SNSP113 significantly reduced the goblet cell metaplasia and epithelial thickening present in the Scnn1b-Tg mouse lung, highlighting the potential for SNSP113 or entities with similar mechanisms to improve the lung pathology

that follows and exacerbates muco-obstructive diseases. Comparable studies have shown that amiloride, hypertonic saline, and more recently, a thiol-saccharide mucolytic (MUC-031) significantly prevent intraluminal mucus accumulation in neonatal Scnn1b-Tg mice, and that 7% hypertonic saline and MUC-301 were able to significantly resolve intraluminal accumulation in adult mice (35, 37, 38). Interestingly, none of these studies reported showed resolution of intraepithelial mucus accumulation, a metric of goblet cell metaplasia, in adult mice, whereas this study showed a decrease in goblet cell metaplasia, possibly due to the distinct mechanism of SNSP113 compared to other mucolytic strategies. Future studies should evaluate SNSP113 efficacy on the prevention of mucus plugging and goblet cell metaplasia in the Scnn1b-Tg model to evaluate the distinct mechanism of mucin polymer correction by SNP113 rather than hydration augmentation or polymer reduction on the prevention of mucus pathology. Additionally, future studies could also include evaluation in CF disease models more affected by mucus obstruction, such as CF pigs, ferrets, or sheep.

ECP is a spontaneous pulmonary lesion that occurs in some strains of mice, notably mice derived from a C57BL/6 background, and increases in prevalence with age (30). ECP is characterized by lung consolidation of the bronchi and alveolar spaces resulting from the infiltration of acidic macrophages and eosinophils and hallmarked by acicular crystal formation within these cells (29, 30, 39). When comorbid with pulmonary diseases that prevent proper airway clearance, these infiltrates accumulate and can lead to decreased respiratory function and morbidity (30). The formation of eosinophilic crystals within mucus plugs and macrophages has been reported previously in juvenile Scnn1b-Tg mice (24). Interestingly, the severity of ECP observed in our study has yet to be reported in Scnn1b-Tg mice, likely because the majority of studies have been performed in juvenile mice, whereas the study reported here utilized mice at least 16 weeks of age. Interestingly, we observed a significant number of Scnn1b-Tg mice with ECP, and that SNSP113 reversed ECP occurrence and lung consolidation to rates seen in WT mice (Figure 4A–E). The occurrence of ECP in adult mice provided a unique opportunity to evaluate the efficacy of SNSP113 in resolving severe inflammation caused by impaired MCC. Consistent with our resolution of ECP after SNSP113 treatment, total WBC and macrophage counts were elevated in vehicle-treated Scnn1b-Tg mice and reduced after SNSP113 treatment. While SNSP113 improved ECP and macrophage influx, elevated neutrophil infiltration in BALF was not resolved (Figure 4H, SI Figure 2E,F), likely due to the way these inflammatory responses manifest over time. Neutrophilia has been well characterized in Scnn1b-Tg mice as chronic and occurring parallel to mucus-obstruction and goblet cell metaplasia (20). ECP occurs secondary to impaired clearance; therefore, improvements to MCC by SNSP113 may have enabled the resolution of ECP relatively quickly, within the 7-day treatment period, whereas long-term improvements in neutrophilic inflammation may require more sustained treatment (30). This will require additional studies to confirm. Overall, the resolution of ECP and macrophage influx by SNSP113 shows that it has beneficial effects on inflammation associated with impaired mucus clearance.

5. Conclusion

In summary, we demonstrated that SNSP113 improves mucus transport and lung pathology in Scnn1b-Tg mice, where mucus stasis occurs consequent to airway dehydration due

to sodium depletion of the airway surface, rather than absent bicarbonate transport through CFTR-mediated secretion. The ability of SNSP113 to improve mucus transport independently from hydration in the Scnn1b-Tg model indicates that SNSP113 can improve mucus viscoelasticity in cases where mucus obstruction results from airway dehydration. This expands the potential of SNSP113 to muco-obstructive diseases beyond CF, such as non-CF bronchiectasis or chronic bronchitis where the promotion of normal MUC5B structure and function could aid airway clearance.

Supplementary Material

Refer to Web version on PubMed Central for supplementary material.

Funding Sources:

Work was supported by the National Institutes of Health [NHLBI, grant numbers 1R35HL135816-01, 5T32HL134640-04, P30DK072482] and the Cystic Fibrosis Foundation [grant number ROWE19RO].

Declarations of interest:

SMR received grant funding and consulting fees from Synspira and Synedgen that ended in 2022. A full list of disclosures is available online. Shenda M. Baker provided SNSP113 (PAAG) used in study. Elex S. Harris, Lea Novak, Courtney M. Fernandez-Petty, and Susan E. Birket have no conflicts of interest to report.

Abbreviations

CF	Cystic fibrosis
MCC	Mucociliary clearance
Ca^{2+}	Calcium
Na^{+}	Sodium
PAAG	Poly (acetyl, arginyl) glucosamine
Tg	Transgenic
βENac	β subunit of the epithelial Na+ channel
μOCT	micro-optical coherence tomography
ASL	Airway surface liquid
PCL	Periciliary liquid
MCT	Mucociliary transport
BALF	Bronchoalveolar lavage fluid
H&E	hematoxylin and eosin
AB-PAS	Alcian blue-periodic acid Schiff's
ECP	Eosinophilic crystalline pneumonia

MPO	Myeloperoxidase
WT	Wild-type
PMN	Polymorphonuclear neutrophils
WBC	white blood cell

References

1. Boyton RJ, Altmann DM. Muco-Obstructive Lung Diseases. N Engl J Med. 2019;381(10):e20.
2. Fahy JV, Dickey BF. Airway mucus function and dysfunction. N Engl J Med. 2010;363(23):2233–47. [PubMed: 21121836]
3. Lamblin G, Degroote S, Perini JM, Delmotte P, Scharfman A, Davril M, et al. Human airway mucin glycosylation: a combinatory of carbohydrate determinants which vary in cystic fibrosis. Glycoconj J. 2001;18(9):661–84. [PubMed: 12386453]
4. Ridley C, Thornton DJ. Mucins: the frontline defence of the lung. Biochem Soc Trans. 2018;46(5):1099–106. [PubMed: 30154090]
5. Thornton DJ, Rousseau K, McGuckin MA. Structure and function of the polymeric mucins in airways mucus. Annu Rev Physiol. 2008;70:459–86. [PubMed: 17850213]
6. Thornton DJ, Sharpe C, Ridley C. Intracellular Processing of Human Secreted Polymeric Airway Mucins. Ann Am Thorac Soc. 2018;15(Suppl 3):S154–S8. [PubMed: 30431345]
7. Verdugo P, Deyrup-Olsen I, Aitken M, Villalon M, Johnson D. Molecular mechanism of mucin secretion: I. The role of intragranular charge shielding. J Dent Res. 1987;66(2):506–8. [PubMed: 3476567]
8. Gustafsson JK, Ermund A, Ambort D, Johansson ME, Nilsson HE, Thorell K, et al. Bicarbonate and functional CFTR channel are required for proper mucin secretion and link cystic fibrosis with its mucus phenotype. J Exp Med. 2012;209(7):1263–72. [PubMed: 22711878]
9. Quinton PM. Cystic fibrosis: impaired bicarbonate secretion and mucoviscidosis. Lancet. 2008;372(9636):415–7. [PubMed: 18675692]
10. Abdullah LH, Evans JR, Wang TT, Ford AA, Makhov AM, Nguyen K, et al. Defective postsecretory maturation of MUC5B mucin in cystic fibrosis airways. JCI Insight. 2017;2(6):e89752. [PubMed: 28352653]
11. Kesimer M, Makhov AM, Griffith JD, Verdugo P, Sheehan JK. Unpacking a gel-forming mucin: a view of MUC5B organization after granular release. Am J Physiol Lung Cell Mol Physiol. 2010;298(1):L15–22. [PubMed: 19783639]
12. Morrison CB, Markovetz MR, Ehre C. Mucus, mucins, and cystic fibrosis. Pediatr Pulmonol. 2019;54 Suppl 3(Suppl 3):S84–S96. [PubMed: 31715083]
13. Hansson GC. Mucus and mucins in diseases of the intestinal and respiratory tracts. J Intern Med. 2019;285(5):479–90. [PubMed: 30963635]
14. Hoegger MJ, Fischer AJ, McMenimen JD, Ostedgaard LS, Tucker AJ, Awadalla MA, et al. Impaired mucus detachment disrupts mucociliary transport in a piglet model of cystic fibrosis. Science. 2014;345(6198):818–22. [PubMed: 25124441]
15. Mall MA, Danahay H, Boucher RC. Emerging Concepts and Therapies for Mucoobstructive Lung Disease. Ann Am Thorac Soc. 2018;15(Suppl 3):S216–S26. [PubMed: 30431343]
16. Fernandez-Petty CM, Hughes GW, Bowers HL, Watson JD, Rosen BH, Townsend SM, et al. A glycopolymer improves vascoelasticity and mucociliary transport of abnormal cystic fibrosis mucus. JCI Insight. 2019;4(8).
17. Birket SE, Davis JM, Fernandez CM, Tuggle KL, Oden AM, Chu KK, et al. Development of an airway mucus defect in the cystic fibrosis rat. JCI Insight. 2018;3(1).
18. Sun X, Sui H, Fisher JT, Yan Z, Liu X, Cho HJ, et al. Disease phenotype of a ferret CFTR-knockout model of cystic fibrosis. J Clin Invest. 2010;120(9):3149–60. [PubMed: 20739752]

19. Schneider CP, Shukla D, Trout BL. Arginine and the Hofmeister Series: the role of ion-ion interactions in protein aggregation suppression. J Phys Chem B. 2011;115(22):7447–58. [PubMed: 21568311]
20. Zhou Z, Duerr J, Johannesson B, Schubert SC, Treis D, Harm M, et al. The ENaC-overexpressing mouse as a model of cystic fibrosis lung disease. J Cyst Fibros. 2011;10 Suppl 2:S172–82. [PubMed: 21658636]
21. Mall M, Grubb BR, Harkema JR, O'Neal WK, Boucher RC. Increased airway epithelial Na+ absorption produces cystic fibrosis-like lung disease in mice. Nat Med. 2004;10(5):487–93. [PubMed: 15077107]
22. Liu L, Chu KK, Houser GH, Diephuis BJ, Li Y, Wilsterman EJ, et al. Method for quantitative study of airway functional microanatomy using micro-optical coherence tomography. PLoS One. 2013;8(1):e54473. [PubMed: 23372732]
23. Birket SE, Chu KK, Liu L, Houser GH, Diephuis BJ, Wilsterman EJ, et al. A functional anatomic defect of the cystic fibrosis airway. Am J Respir Crit Care Med. 2014;190(4):421–32. [PubMed: 25029666]
24. Mall MA, Harkema JR, Trojanek JB, Treis D, Livraghi A, Schubert S, et al. Development of chronic bronchitis and emphysema in beta-epithelial Na+ channel-overexpressing mice. Am J Respir Crit Care Med. 2008;177(7):730–42. [PubMed: 18079494]
25. Dinwiddie R. Pathogenesis of lung disease in cystic fibrosis. Respiration. 2000;67(1):3–8. [PubMed: 10705255]
26. De Rose V, Molloy K, Gohy S, Pilette C, Greene CM. Airway Epithelium Dysfunction in Cystic Fibrosis and COPD. Mediators Inflamm. 2018;2018:1309746. [PubMed: 29849481]
27. Ma J, Rubin BK, Voynow JA. Mucins, Mucus, and Goblet Cells. Chest. 2018;154(1):169–76. [PubMed: 29170036]
28. Livraghi A, Grubb BR, Hudson EJ, Wilkinson KJ, Sheehan JK, Mall MA, et al. Airway and lung pathology due to mucosal surface dehydration in beta-epithelial Na+ channel-overexpressing mice: role of TNF-alpha and IL-4Ralpha signaling, influence of neonatal development, and limited efficacy of glucocorticoid treatment. J Immunol. 2009;182(7):4357–67. [PubMed: 19299736]
29. Murray AB, Luz A. Acidophilic macrophage pneumonia in laboratory mice. Vet Pathol. 1990;27(4):274–81. [PubMed: 2169666]
30. Klug JJ, Snyder JM. Eosinophilic crystalline pneumonia, an age-related lesion in mice. Aging Pathobiol Ther. 2020;2(4):232–3. [PubMed: 35028642]
31. Rowe SM, Miller S, Sorscher EJ. Cystic fibrosis. N Engl J Med. 2005;352(19):1992–2001. [PubMed: 15888700]
32. Ehre C, Rushton ZL, Wang B, Hothem LN, Morrison CB, Fontana NC, et al. An Improved Inhaled Mucolytic to Treat Airway Muco-obstructive Diseases. Am J Respir Crit Care Med. 2019;199(2):171–80. [PubMed: 30212240]
33. Mall MA, Graeber SY, Stahl M, Zhou-Suckow Z. Early cystic fibrosis lung disease: Role of airway surface dehydration and lessons from preventive rehydration therapies in mice. Int J Biochem Cell Biol. 2014;52:174–9. [PubMed: 24561284]
34. Pieper M, Schulz-Hildebrandt H, Mall MA, Huttmann G, Konig P. Intravital microscopic optical coherence tomography imaging to assess mucus-mobilizing interventions for muco-obstructive lung disease in mice. Am J Physiol Lung Cell Mol Physiol. 2020;318(3):L518–L24. [PubMed: 31994896]
35. Addante A, Raymond W, Gitlin I, Charbit A, Orain X, Scheffler AW, et al. A novel thiol-saccharide mucolytic for the treatment of muco-obstructive lung diseases. Eur Respir J. 2023;61(5).
36. Walker NM, Liu J, Young SM, Woode RA, Clarke LL. Goblet cell hyperplasia is not epithelial-autonomous in the Cftr knockout intestine. Am J Physiol Gastrointest Liver Physiol. 2022;322(2):G282–G93. [PubMed: 34878935]
37. Zhou Z, Treis D, Schubert SC, Harm M, Schatterny J, Hirtz S, et al. Preventive but not late amiloride therapy reduces morbidity and mortality of lung disease in betaENaC-overexpressing mice. Am J Respir Crit Care Med. 2008;178(12):1245–56. [PubMed: 18849497]

38. Graeber SY, Zhou-Suckow Z, Schatterny J, Hirtz S, Boucher RC, Mall MA. Hypertonic saline is effective in the prevention and treatment of mucus obstruction, but not airway inflammation, in mice with chronic obstructive lung disease. Am J Respir Cell Mol Biol. 2013;49(3):410–7. [PubMed: 23590312]

39. Hoenerhoff MJ, Starost MF, Ward JM. Eosinophilic crystalline pneumonia as a major cause of death in 129S4/SvJae mice. Vet Pathol. 2006;43(5):682–8. [PubMed: 16966445]

Highlights:

- SNSP113 significantly improved MCT in a Scnn1b-Tg mouse model of mucus stasis.
- SNSP113 corrected MCT independent of airway hydration in Scnn1b-Tg mice.
- SNSP113 reduced and epithelial hypertrophy in Scnn1b-Tg mice.
- SNSP113 reduced incidence of eosinophilic crystalline pneumonia in Scnn1b-Tg mice.
- SNSP113 and other agents may have beneficial effects in diseases mucus stasis associated with malformation of mucins.

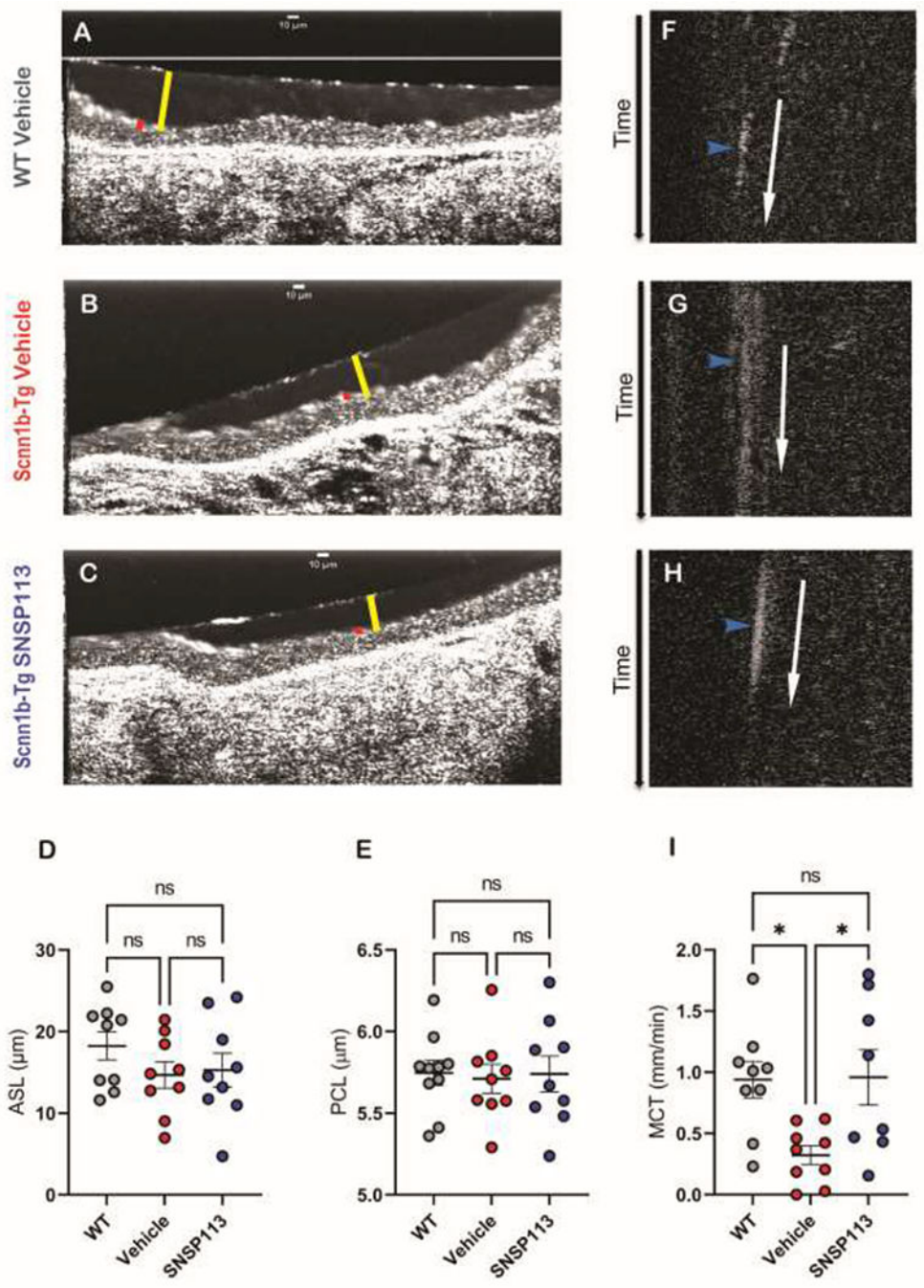

Figure 1. SNSP113 restores mucus transport in Scnn1b-Tg mice without impacting airway hydration.

(A-C) Representative µOCT images of trachea excised from **(A)** WT mice treated with 1.38% glycerol in PBS vehicle and Scnn1b-Tg mice treated with either **(B)** 1.38% glycerol in PBS vehicle or **(C)** 250 µg/mL SNSP113 1.38% glycerol in PBS demonstrate no differences in ASL (yellow bar) or PCL (red bar). Summary data of **(D)** ASL and **(E)** PCL depth. Time-dependent reprocessed image show tracks of mucus particles above the epithelial surface of **(F)** WT mice treated with 1.38% glycerol in PBS vehicle and

Scnn1b-Tg mice treated with either **(G)** 1.38% glycerol in PBS vehicle or **(H)** 250 μg/mL SNSP1131.38% glycerol in PBS; the more horizontal direction of particle streaks (blue arrow) indicates more rapid transport. **(I)** Summary data shows effect of SNSP113 on MCT. Regions of interest were measured and averaged for each animal for (D) ASL, (E) PCL, (I) MCT. N=9/condition. nsP>0.05, *P<0.05 by Kruskal Wallis test comparing mean ranks. Scale bars, 10μm.

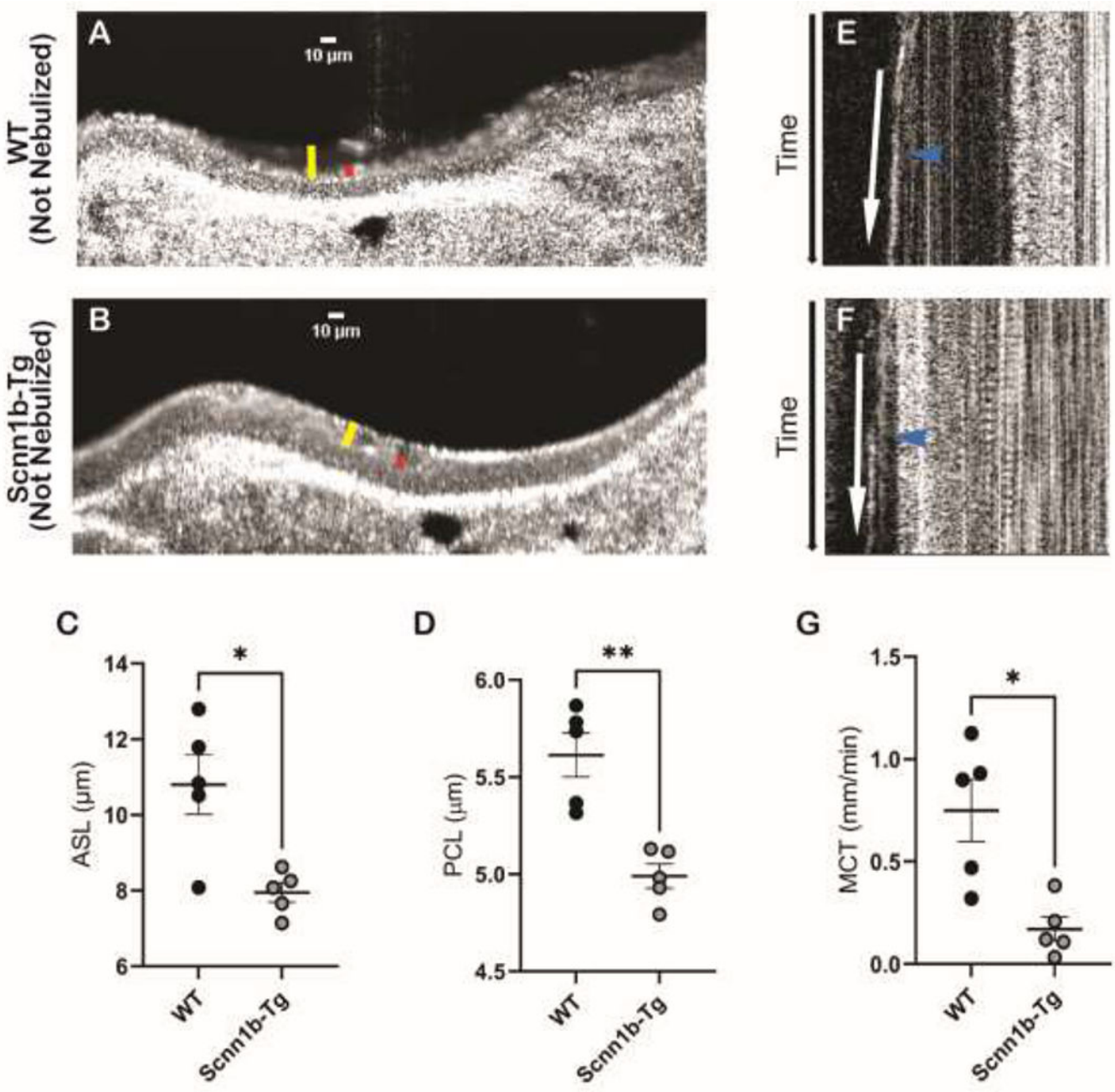

Figure 2. Scnn1b-Tg mice exhibit a deficit in ASL and PCL prior to nebulization.

(A-B) Representative μOCT images of trachea excised from **(A)** WT mice and **(B)** Scnn1b-Tg mice without any treatment demonstrate a reduced ASL (yellow bar) and PCL (red bar) in Scnn1b-Tg mice. Summary data of **(C)** ASL and **(D)** PCL depth. Time-dependent reprocessed images show tracks of mucus particles above the epithelial surface of **(E)** WT mice and **(F)** Scnn1b-Tg mice without any treatment; the more horizontal direction of particle streaks (blue arrow) indicates more rapid transport. **(G)** Summary data highlights reduced MCT in Scnn1b-Tg mice. Regions of interest were measured and averaged for each

animal for (C) ASL, (D) PCL, (G) MCT. N=5/condition. N=9/condition. *P<0.05, **P<0.01 by Kruskal Wallis test comparing mean ranks. Scale bars, 10μm.

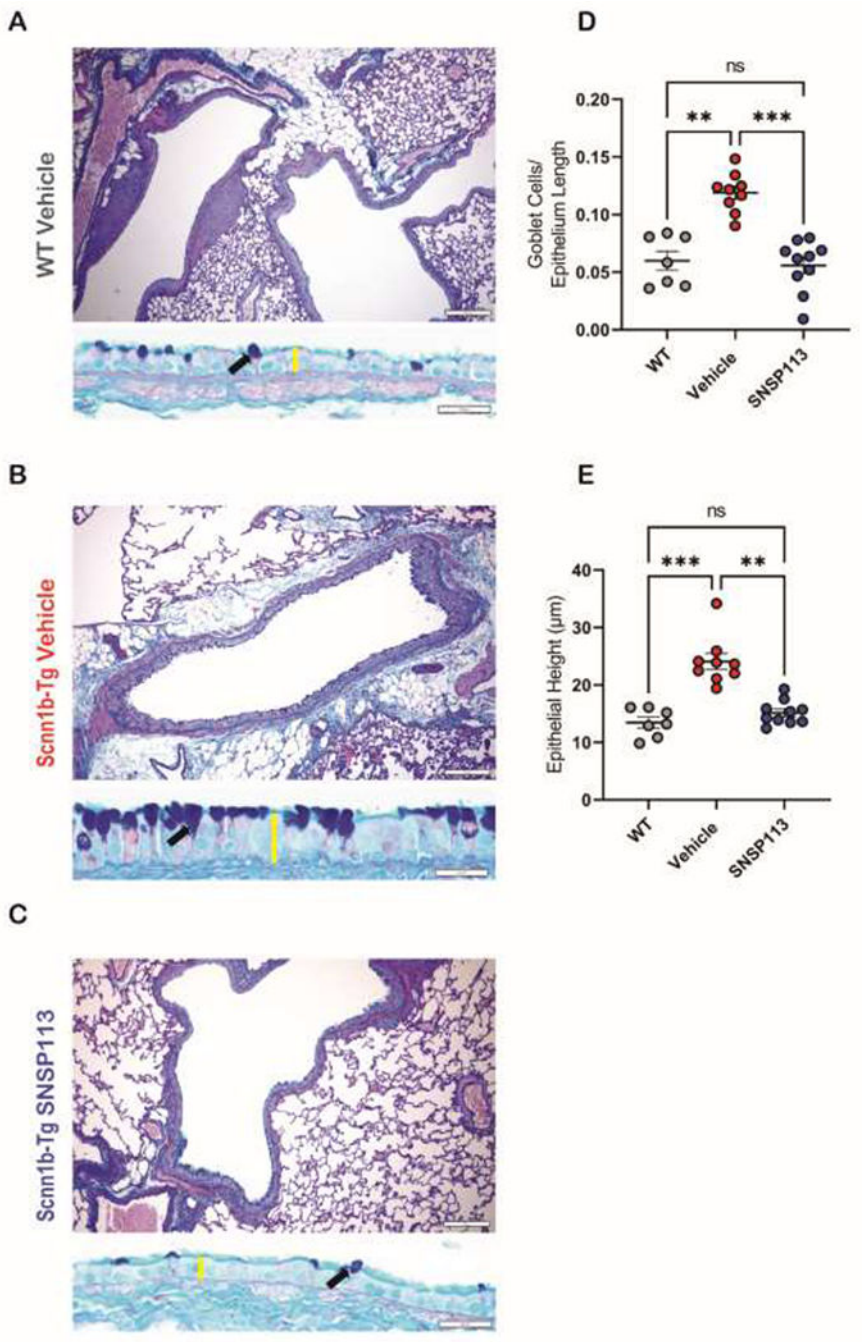

Figure 3. SNSP113 reduces goblet cell metaplasia and epithelial hypertrophy in the airways of Scnn1b-Tg mice.

(A-C) Representative AB-PAS stained airways highlight differences in goblet cell metaplasia (black arrow) and epithelial height (yellow bar) between **(A)** WT mice treated with 1.38% glycerol in PBS vehicle compared to Scnn1b-Tg mice treated with either **(B)** 1.38% glycerol in PBS vehicle or **(C)** S 250 μg/mL.1.38% glycerol in PBS. Summary data of **(D)** number of goblet cells per mm of epithelium length and **(E)** height of

epithelium (μm). N=7-10/condition. nsP>0.05, **P<0.01, ***P<0.001 by Kruskal Wallis test comparing mean ranks. Scale bars, 100um and 20μm, respectively.

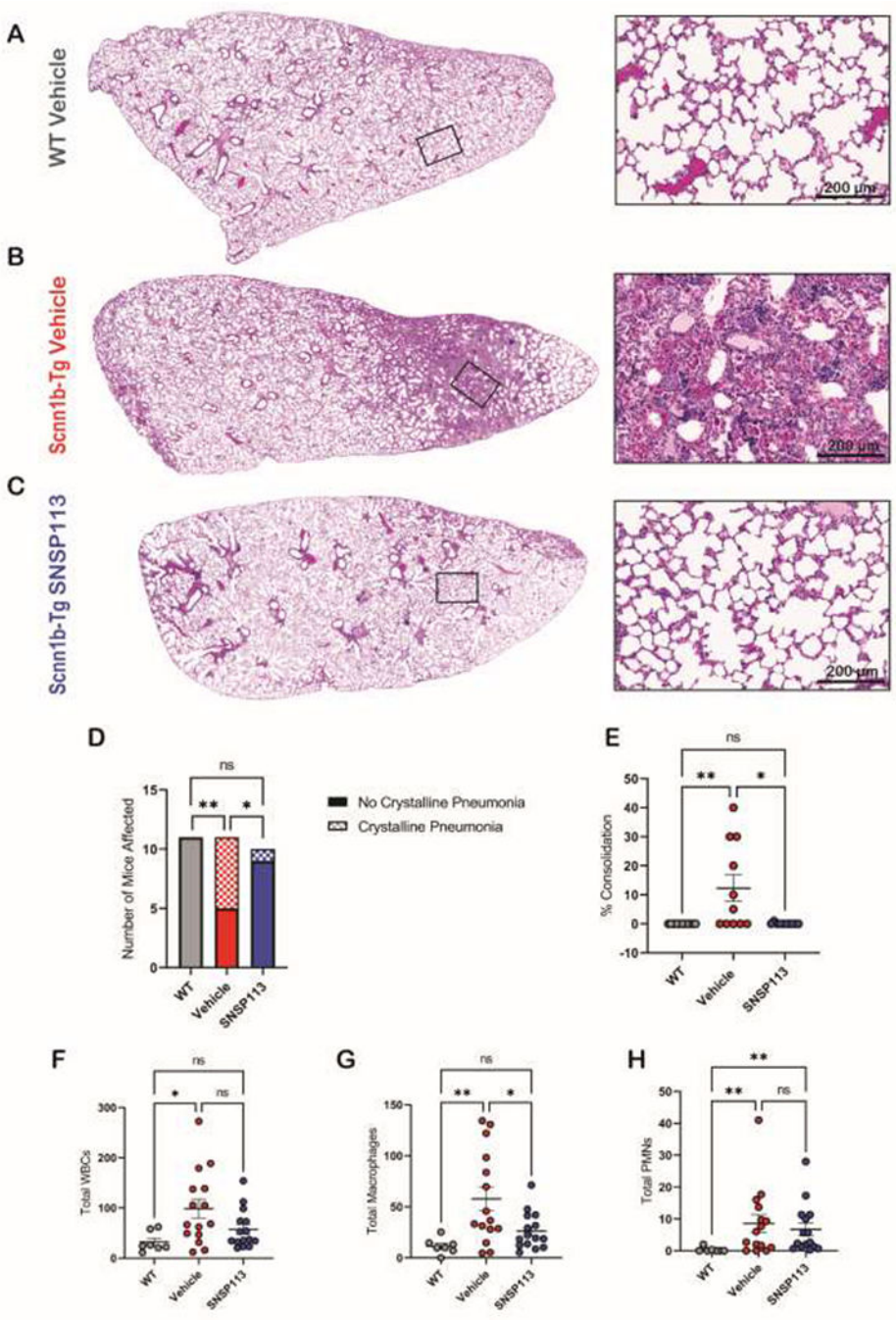

Figure 4. SNSP113 reduces incidence of eosinophilic crystalline pneumonia (ECP) in the Scnn1b-Tg mouse.

(A-C) H&E-stained lung sections (magnification 100X and 400X) show normal lungs in **(A)** WT mice treated with 1.38% glycerol in PBS vehicle compared to severe ECP in Scnn1b-Tg mice that treated with **(B)** 1.38% glycerol in PBS vehicle, which is substantially resolved in **(C)** Scnn1b-Tg mice treated with 250ug/mL SNSP113. **(D-E)** Quantification of animals show presence of ECP and percent of ECP lung consolidation highlight the resolution of ECP after SNSP113 treatment. N=10 to 11/condition. nsP>0.05, *P<0.05, **P<0.01 by Chi

Square or Kruskal Wallis test comparing mean ranks, respectively. Scale bars, 200μm. **(F)** Total WBC counts in BALF samples and differential counts of **(G)** total macrophages and **(H)** total PMNs in the BALF samples of WT mice treated with 1.38% glycerol in PBS vehicle and Scnn1b-Tg mice treated with either 1.38% glycerol in PBS vehicle or 250ug/mL SNSP113.1.38% glycerol in PBS N=7 to 15/condition. nsP>0.05, *P<0.05, **P<0.01 by Ordinary one-way ANOVA or Kruskal Wallis test as appropriate.